https://doi.org/10.5194/egusphere-2026-3486
Preprint. Discussion started: 25 June 2026

Temporal variability in offshore Fe fluxes in the Peruvian oxygen minimum zone across an El Niño termination

Guanghui Chen[1], Insa Rapp[2], Matthias Sieber[3,4], Eric P. Achterberg[2], Tim M. Conway[3], Martha Gledhill[2], Mark J. Hopwood[2,5], Ruifang C. Xie[1,2,6]

[1] State Key Laboratory of Submarine Geoscience and School of Oceanography, Shanghai Jiao Tong University, Shanghai, 200030, China.
[2] GEOMAR Helmholtz Centre for Ocean Research, Kiel, 24148, Germany
[3] College of Marine Science, University of South Florida, St. Petersburg, 33701, USA
[4] Department of Earth and Planetary Sciences, ETH Zürich, Zürich, 8092, Switzerland
[5] Department of Ocean Science and Engineering, Southern University of Science and Technology, Shenzhen, 518055, China
[6] Key Laboratory for Polar Science, Polar Research Institute of China, Ministry of Natural Resources, Shanghai, 200136, China

Correspondence to: Ruifang C. Xie (ruifang.xie@sjtu.edu.cn)

Abstract. Offshore fluxes of Fe in the Peruvian oxygen minimum zone are sensitive to seawater redox state, and potentially modulated by the El Niño-Southern Oscillation. However, observational data on what controls such temporal variation in offshore Fe fluxes remain scarce. Here, we report seawater concentrations of dissolved Fe (dFe), particulate Fe (pFe), and their isotopic compositions (δ^{56}dFe and δ^{56}pFe) from two transects at 12°S and 14°S across the Peruvian shelf. Our data show clear shelf-to-slope dFe and pFe plumes with negative δ^{56}Fe signatures. Maximum Fe concentrations at 12°S decreased from 13 to 4 nmol kg^{-1} (dFe) and 122 to 13 nmol kg^{-1} (pFe) over a month across an El Niño event termination. We link these variations to an intensifying Peru-Chile Undercurrent which enhanced oxygen supply and thereby weakened sedimentary reductive Fe effluxes. Off shelf, elevated δ^{56}dFe and low δ^{56}pFe in anoxic waters are attributed to organic ligand binding and authigenic Fe formation.

1 Introduction

Iron (Fe) is an essential micronutrient for marine organisms, playing a critical role in photosynthesis, respiration and N_2 fixation (Morel and Price, 2003; Whitfield, 2001). The availability of Fe limits primary production in most upwelling regions owing to the deficient supply of Fe relative to macronutrients (Browning and Moore, 2023). Peruvian shelf waters are characterized by coastal upwelling that brings nutrient-rich deep waters to the surface (Chavez and Messié, 2009), promoting primary production and supporting the world's largest fishery (Pauly and Christensen, 1995). However, residual nitrate in the photic zone and incubation experiments both indicate that phytoplankton growth in the Peruvian upwelling zone is limited by Fe availability (Hutchins et al., 2002; Browning et al., 2018).

Dissolved Fe (dFe) in Peruvian shelf waters is dominantly derived from reductive dissolution of sediments (Chever et al., 2015). Peruvian shelf waters are anoxic (dissolved oxygen (DO) < 2 μmol kg^{-1}) below the mixed layer due to organic matter remineralization and sluggish ventilation (Karstensen et al., 2008). The Peruvian oxygen minimum zone (OMZ) extends from

https://doi.org/10.5194/egusphere-2026-3486
Preprint. Discussion started: 25 June 2026

the mixed-layer (~50 m) down to ~500 m, resulting in a wide aera of shelf sediments overlain by anoxic waters (Noffke et al., 2012; Scholz et al., 2016). Anoxic porewaters promote the reductive dissolution of sedimentary ferric Fe (Fe(III)) and thereby the accumulation of dissolved ferrous Fe (Fe^{2+}) in porewater (Noffke et al., 2012; Scholz et al., 2014). Subsequently, dissolved Fe^{2+} diffuses upward, where it can cross the sediment-water interface and increase dFe concentrations in the Peruvian shelf bottom waters (Schlosser et al., 2018). Sediment-derived Fe(II) (refer to Fe(II) that is supplied from reducing sediments thereafter) is then steadily re-oxidized within the Peruvian OMZ to Fe(III), though notably slower than under oxic conditions, either via trace amounts of DO, H_2O_2, or by denitrifying microbes during dissimilatory nitrate reduction (Scholz et al., 2016; Heller et al., 2017; Miller et al., 1995). Conversely, when porewater in the upper few cm of shelf sediments is oxic, or the overlying water column is oxic, Fe(III) rapidly precipitates as Fe (oxyhydr)oxides. Under these conditions, benthic Fe effluxes are low (Liu and Millero, 2002; Severmann et al., 2010). In shelf regions, DO concentrations in the water column are therefore key regulators of benthic dFe effluxes (Noffke et al., 2012). A plume of sediment-derived dFe from the inner shelf is often laterally exported to the open ocean within the anoxic water column through offshore currents, a process known as the "open marine Fe shuttle" (Scholz et al., 2014; Noffke et al., 2012).

This shelf-to-slope dFe export is thought to be strongly influenced by El Niño events during which dFe concentrations over the shelf drop by orders of magnitude due to oxygenation of the water column (Scholz et al., 2011; Rapp et al., 2020). El Niño and La Niña are opposing phases of the El Niño-Southern Oscillation (ENSO) characterized by variations in sea surface temperatures across the Equatorial Pacific. During the El Niño events, which are intense warm phases of ENSO, the thermocline, nutricline and oxycline deepen. The lateral supply of subtropical-sourced DO is enhanced (José et al., 2019), and the intensity of upwelling in eastern tropical Pacific declines (Espinoza-Morriberón et al., 2017) resulting in reduced primary production (Stramma et al., 2016). Conversely, during La Niña events, which are extreme cold phases of ENSO, lateral transportation of oxygenated subtropical waters is reduced, and a shallower nutricline, oxycline, and thermocline lead to enhanced upwelling of nutrient-rich waters facilitating higher primary production and subsurface water deoxygenation (Carr, 2003, Espinoza-Morriberón et al., 2017, José et al., 2019). Dissolved Fe concentrations close to the coastline respond rapidly to ENSO dynamics (Gu et al., 2024). Under La Niña events, anoxic shelf waters promote dFe release into the water column, whereas El Niño events drive oxic shelf waters which promotes Fe(III) precipitation in bottom waters (Scholz et al., 2011). However, dFe concentrations in the water column across the inner Peruvian shelf vary within a broad range (1-50 nmol kg^{-1}) even within specific ENSO phases (Gu et al., 2024). Spatial and temporal variability in dFe concentrations over the Peruvian shelf also reflects varying shelf width, productivity and mesoscale dynamics (Rapp et al., 2020; Bruland et al., 2005).

Fe isotopes are a useful tracer for Fe inputs from shelf sediments (John et al., 2012; Homoky et al., 2021; Fitzsimmons and Conway, 2023). Oxic sediments supply dFe with Fe isotopic composition (δ^{56}Fe) equivalent to the crustal value of +0.1‰ (Beard et al., 2003; Homoky et al., 2021). In contrast, under low oxygen conditions and in OMZs, reductive dissolution of shelf sediments contributes dissolved Fe^{2+} to sediment porewaters (Froelich et al., 1979) with δ^{56}dFe ranging from −3.5 to −1.5‰ (e.g. Severmann et al., 2006; Homoky et al., 2009; Homoky et al., 2013; Severmann et al., 2010; Klar et al., 2017). This low δ^{56}dFe signatures can be observed in overlying bottom waters (e.g. John et al., 2012; Klar et al., 2017). The δ^{56}Fe

https://doi.org/10.5194/egusphere-2026-3486
Preprint. Discussion started: 25 June 2026

difference between seawater and porewater has thus been used to distinguish sedimentary dFe input (e.g. Conway and John, 2014; Chever et al., 2015; Klar et al., 2017; John et al., 2018; Hunt et al., 2022; Tian et al., 2023, 2026). On the Peruvian shelf, δ^{56}dFe as low as −1.25‰ has been reported, coupled with elevated Fe(II) concentrations (Vedamati et al., 2014; Chever et al., 2015). The reductive signatures of δ^{56}dFe have been reported to persist for the duration of shelf-to-basin scale transport and even over thousands of kilometers (Sieber et al., 2021, 2024; Hunt, 2025; Camin et al., 2026). Previous studies from Peru have observed a shelf-to-slope transport of sediment-derived dFe driven by the marine iron shuttle (John et al., 2018; Heller et al., 2017), which may generate a broader slope dFe plume proceeding ~4000 km offshore (John et al., 2018). How the iron shuttle influences particulate Fe and its isotopic composition remains less clear.

In this study, we present a unique dataset of Fe concentrations and Fe isotope ratios for the dissolved and particulate phases from 0-2000 m in the Peruvian OMZ during a post-El Niño period, that is, a period immediately following the end of an El Niño event. We link variations of these parameters to Fe(II) dynamics in order to investigate short-term variability, over time scales of less than 1 month, in the reductive release of dFe from Peruvian shelf sediments, and the extent of dFe and pFe offshore transport to the open ocean.

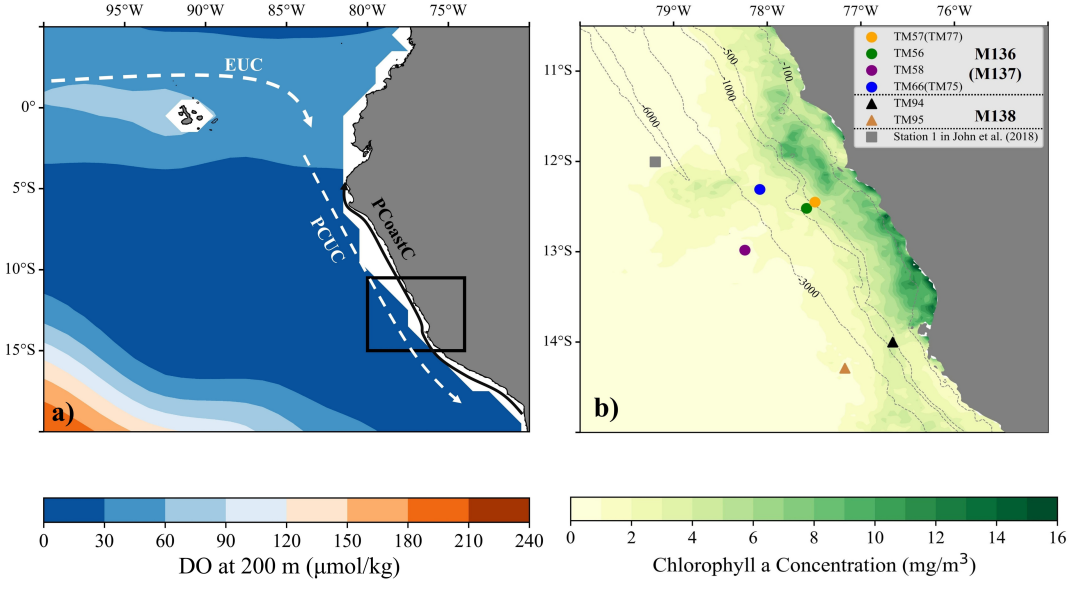

Figure 1. Charts of the Peruvian Upwelling region. **a)** Average dissolved oxygen concentration at the depth of 200 m over 1971 to 2000, derived from Word Ocean Atlas 2023 (Garcia et al., 2024). The dashed lines represent the subsurface Equatorial Undercurrent (EUC) and Peru-Chile Undercurrent (PCUC). The solid line represents Peru Coastal Current (PCoastC). The rectangle highlights the sampling area. **b)** Zoom-in map showing sampling stations from M136, M137 and M138. Crossover stations TM66 and TM75, TM57 and TM77 were located at the same sites but sampled on different cruises. The square delineates Station 1 in John et al. (2018). Concentrations of chlorophyll a were downloaded from NASA Ocean Color (https://oceandata.sci.gsfc.nasa.gov/).

https://doi.org/10.5194/egusphere-2026-3486
Preprint. Discussion started: 25 June 2026

2 Materials and Methods

A total of 8 stations were sampled at depths of 0 to 2000 m along two shelf-slope transect at 12°S and 14°S during three cruises (M136, M137, M1138) in the Peruvian upwelling zone where poleward flowing Peru-Chile Undercurrent (PCUC) dominates in the subsurface layer (50-500 m) (Fig. 1; Chaigneau et al., 2013). The cruises captured the end of an unusual 'coastal' El Niño event in 2017 (Echevin et al., 2018), where El Niño conditions were only experienced in the eastern tropical Pacific, and not basin-wide (Ramírez and Briones, 2017). Cruises M136 captured the termination of the event, and cruises M137 and M138 occurred immediately afterwards. Specifically, stations TM57, TM56, TM58 and TM66 were sampled in the period of 20 April to 1 May 2017 (M136 cruise), with TM66 located in the center of an anticyclonic eddy during sampling. Stations TM57 and TM66 were revisited during cruise M137 (15 to 21 May 2017), identified as the corresponding crossover stations TM77 and TM75. Stations TM 94 and TM95 were sampled on 15 and 16 June 2017 during the M138 cruise. Seawater samples were collected using GO-FLO bottles (Ocean Test Equipment®) mounted on a GEOTRACES compliant trace metal clean rosette or a towed-fish system pumping from a depth of ~2 m. Dissolved samples and particulate samples were obtained through filtration (using 0.2 µm polyethersulfone filters). The dissolved samples for dFe and δ^{56}dFe were immediately acidified to pH ≈ 1.9, and stored double-bagged until further analysis. The filters were stored double-bagged at −20°C until measurements for particulate Fe (pFe), particulate Al (pAl), and pFe isotopic compositions (δ^{56}pFe).

Chemical processing of dissolved and particulate samples was performed in Class-5 trace metal clean laboratories at GEOMAR Helmholtz Centre for Ocean Research, Kiel. All acids used were either of UpA™ grade (Romil®) or distilled with a Savillex® acid purification system. Particulate samples on the filters were digested via refluxing with 10% HF/50% HNO_3 at 150°C for 15 hours. Concentrations of pFe and pAl were analyzed on 10% aliquots of the digest samples on the Element HR-ICP-MS. Iron isotopic compositions were expressed as delta notation relative to the IRMM-014 standard:

$$\delta^{56}Fe(‰) = \left(\frac{(^{56}Fe/^{54}Fe)_{sample}}{(^{56}Fe/^{54}Fe)_{IRMM-014}} - 1 \right) \times 1000 \quad (1)$$

The chemical purification of dissolved and particulate Fe isotopic compositions (δ^{56}dFe and δ^{56}pFe, respectively) were carried out following the methods of Sieber et al. (2021) at ETH Zürich. Analysis of samples was carried out by Neptune Plus MC-ICPMS at the University of South Florida, again following the approach of Sieber et al (2021). Long-term instrumental precision of this method was assessed via multiple analysis of the NIST-3126a standard, yielding an average of +0.36 ± 0.04‰ (2 standard deviations (SD), n = 351; 24 sessions over 3 years), the composition of which agrees well with other studies (Hunt et al., 2022). Accuracy of this analytical method has also been demonstrated by intercalibration efforts (Conway et al., 2016; Kurisu et al., 2024). The uncertainties for δ^{56}Fe used here are the external error (0.04‰); for samples with larger 2SD internal errors, the internal errors were presented. Reported dFe concentrations were calculated from the MC-ICPMS data using the isotopic dilution technique, for which we assign a 2% uncertainty (Conway et al., 2013).

https://doi.org/10.5194/egusphere-2026-3486
Preprint. Discussion started: 25 June 2026

3 Results

3.1 Fe concentrations and Fe isotopic compositions along the 12°S transect

In surface waters, concentrations of dFe and pFe during the M136 cruise were fairly low, always < 0.5 and 1.5 nmol kg^{-1}, respectively (Figs. 2 and 3). Below the oxic-anoxic interface where DO reached below the detection limit of Winkler titrations (2 µmol kg^{-1}), TM57, TM56 and TM58 were influenced by an Fe(II) plume with Fe(II) > 1 nmol kg^{-1}, occupying the depths of 50 to 300 m (neutral density of 26.0 to 26.3 kg m^{-3}) and extending to at least 1° in longitude away from the coast (Fig. 3). In the plume, dFe and pFe concentrations were largely elevated with the maxima occurring at TM57 (closer to the margin). Correspondingly, δ^{56}dFe within the Fe(II) plume was lower, or isotopically lighter (−1.34 to +0.10‰) than values of overlying and subjacent seawater (−0.62 to +0.22‰). Proceeding along the offshore pathway of the Fe(II) plume, over 100 km, the maximal concentrations of dFe and pFe decreased from 13 to 3 nmol kg^{-1}, and from 122 to 7 nmol kg^{-1}, respectively. In parallel, δ^{56}dFe increased from −1.34‰ over the shelf (TM57) to −0.27‰ offshore (TM58) (Fig. 3c). At the eddy station TM66, both dFe and pFe were elevated below the oxic-anoxic interface (~100 m), where concentrations of dFe ranged from 1 to 3 nmol kg^{-1}, while pFe varied from 1 to 17 nmol kg^{-1} (Figs. 2c and 3). In the anoxic layer at TM66 (100-600 m), δ^{56}dFe was higher (−0.05 to +0.73‰) than that (−0.56 to −0.20‰) in suboxic or oxic waters (Fig. 2c).

Clear temporal variations in both dFe and pFe concentrations within the Fe(II) plume were observed on the shelf. Remarkably, the maximum concentrations of dFe and pFe at crossover stations TM57 and TM77 decreased drastically in a ~1 month interval, from 13 and 122 nmol kg^{-1} (M136) to 4 and 13 nmol kg^{-1} (M137), respectively. The corresponding δ^{56}dFe shifted from −1.34‰ during M136 to more elevated values of −0.42‰ during M137 (Figs. 2a and 3c). By contrast, profiles of dFe, pFe and δ^{56}dFe showed no variation within the offshore anticyclonic eddy (between TM66 and TM75). Note that pFe was elevated (9 nmol kg^{-1}) at a depth of 150 m at TM75 but no sample was collected for a direct comparison at the same depth at TM66.

Depth profiles of δ^{56}pFe were obtained at stations TM77, TM56 and TM75 (Fig. 2a, b and c). Values of δ^{56}pFe displayed large variations ranging from −0.89 to +0.93‰. The highest and lowest δ^{56}pFe occurred respectively at the surface and oxic-anoxic interface at the eddy stations. Values of δ^{56}pFe at the sediment-water interface were identical to that of the UCC (−0.01 to +0.19‰) (Beard et al., 2003; Gong et al., 2017).

https://doi.org/10.5194/egusphere-2026-3486
Preprint. Discussion started: 25 June 2026

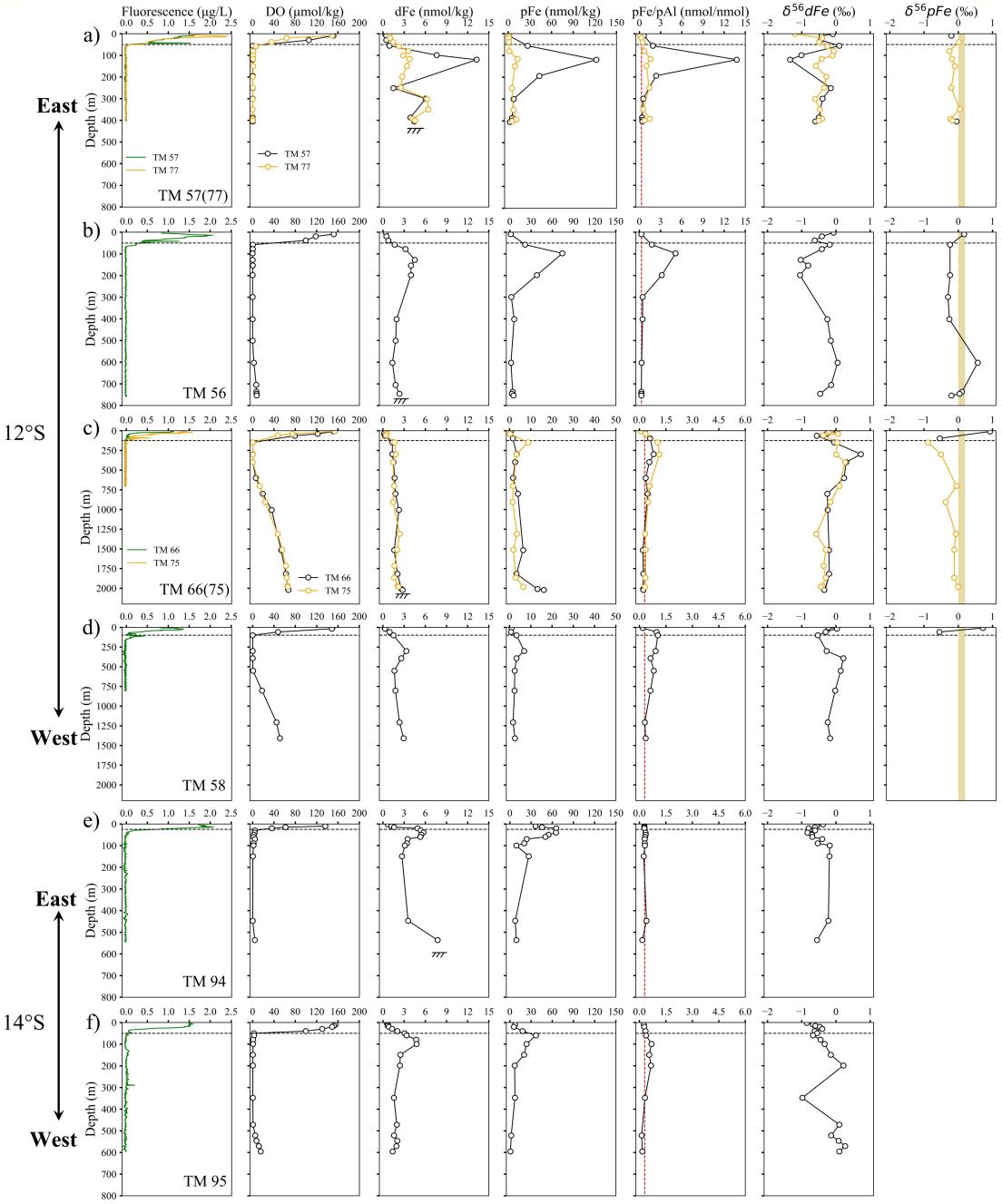

145 **Figure 2.** Depth profiles of fluorescence, DO, dFe, pFe, pFe/pAl, δ^{56}dFe and δ^{56}pFe. Horizontal dashed lines indicate oxic-anoxic interfaces in the water column. Vertical dashed lines indicate the pFe/pAl ratio (0.3 mol: mol) of the andesitic crust endmember (Taylor and McLennan, 1995). The vertical yellow bars represent the δ^{56}Fe signature (−0.01 to +0.19‰) of crust materials (Beard et al., 2003; Gong et al., 2017).

https://doi.org/10.5194/egusphere-2026-3486
Preprint. Discussion started: 25 June 2026

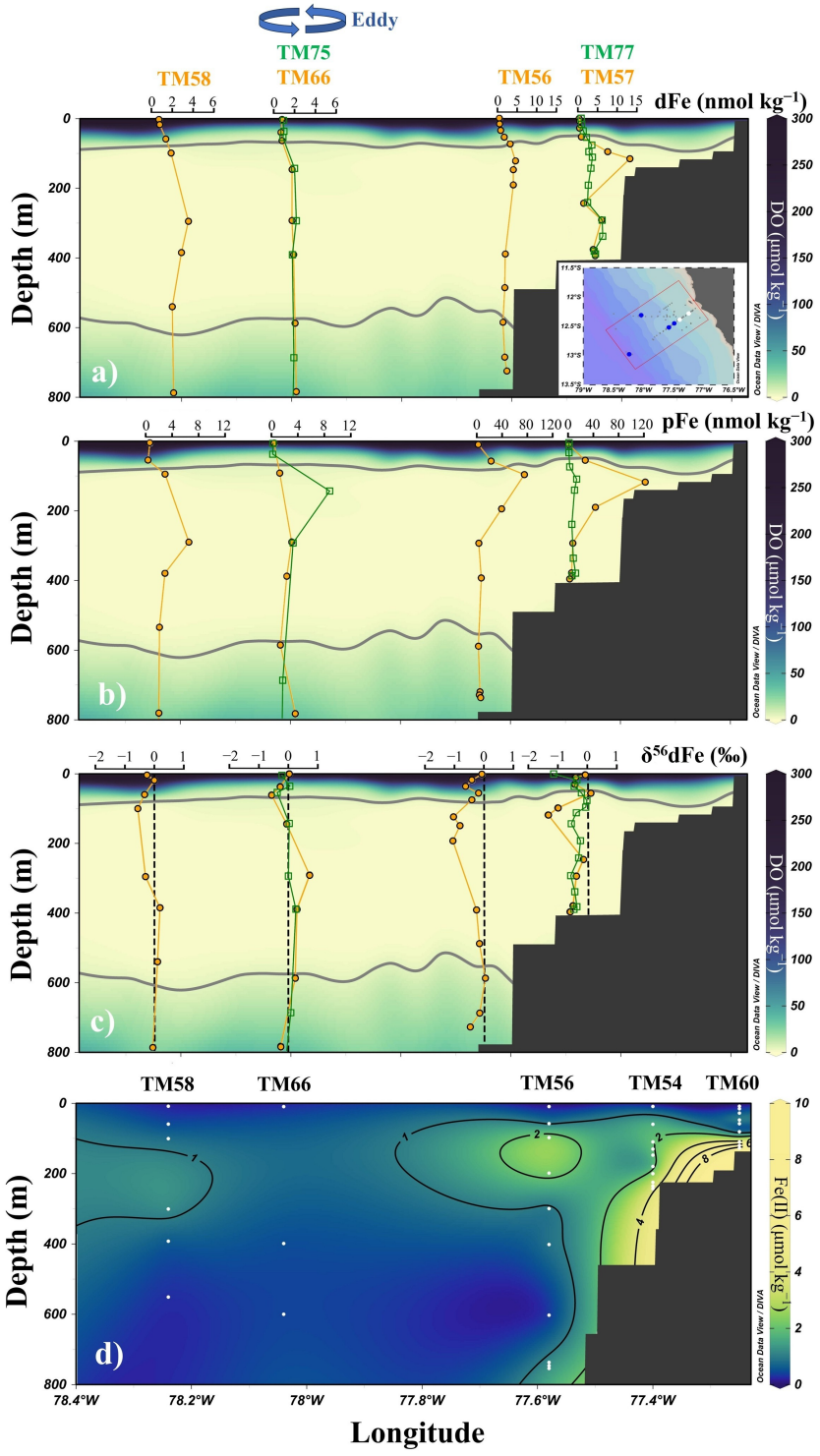

https://doi.org/10.5194/egusphere-2026-3486
Preprint. Discussion started: 25 June 2026

Figure 3. Depth profiles of **a)** dFe, **b)** pFe, **c)** δ^{56}dFe, and **d)** Fe(II) at depths of 0-800 m along the 12°S transect. Dissolved oxygen concentrations are derived from the oxygen sensor mounted on the TM-rosette frame during the M136 cruise. The anoxic layer is annotated using the 2 µmol kg^{-1} DO contours. Data from TM77 and TM75 are represented by green squares to distinguish from TM57 and TM66 which were collected at the same coordinates. Concentrations of Fe(II) are from Zhu et al. (2021). Locations of TM54 and TM60 are indicated by white circles in the inset map in a). Note that data points deeper than 800 m at TM66, TM58 and TM75 are presented in Figure 2. Dashed vertical lines in subplot c) indicate δ^{56}dFe = 0. Location of TM56 in a)-c) is offset for clarity.

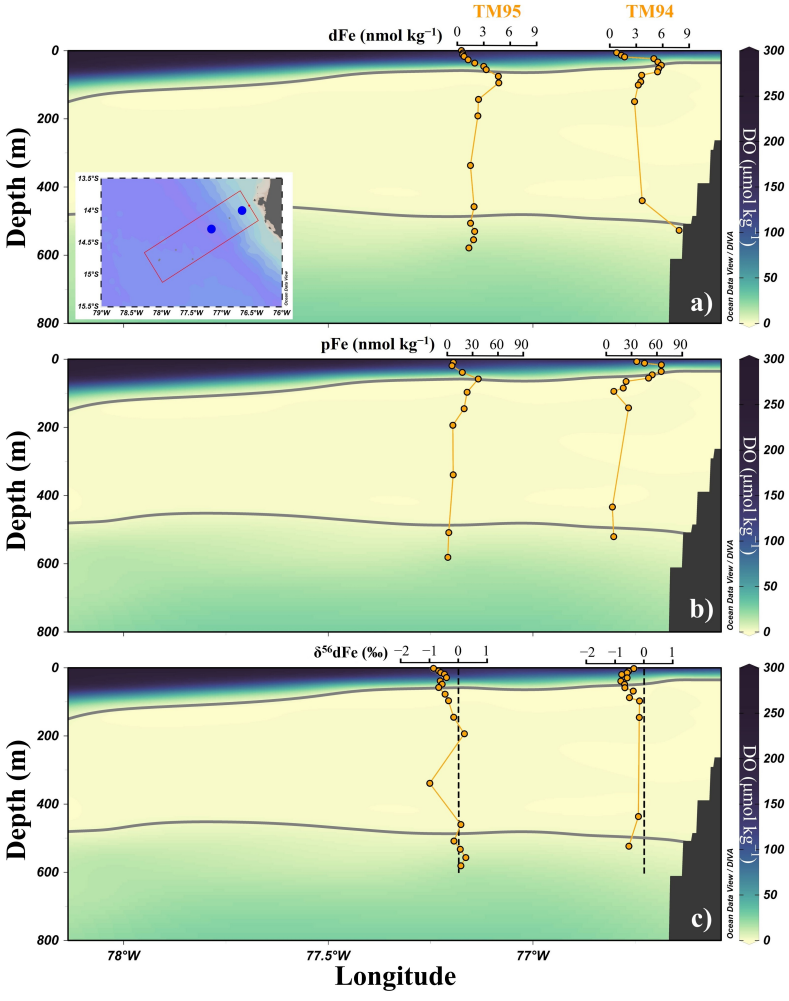

Figure 4. Depth profiles of **a)** dFe, **b)** pFe and **c)** δ^{56}dFe at 14°S transect. Dissolved oxygen concentrations are derived from the oxygen sensor attached to the TM-rosette during M138 cruise. The anoxic layer is annotated using the 2 µmol kg^{-1} DO contours.

3.2 Fe concentrations and Fe isotopic compositions along the 14°S transect

Concentrations of dFe and pFe along the 14°S transect displayed maxima at the oxic-anoxic interface (Figs. 2e, f and 4). The maximum dFe concentration of 5 nmol kg^{-1} at TM94 (the shelf station) was comparable to that at TM95. In contrast, the

https://doi.org/10.5194/egusphere-2026-3486
Preprint. Discussion started: 25 June 2026

maximum pFe concentration of 65 nmol kg^{-1} at TM94 was higher than that at TM95 (37 nmol kg^{-1}). The δ^{56}dFe profile at TM94 mirrored that of dFe, ranging between −0.18‰ and −0.83‰. Values of δ^{56}dFe at TM95 increased from −0.85‰ at the surface to +0.22‰ at the depth of 200 m and remained relatively constant below except for a low δ^{56}dFe occurring at the depth of 350 m.

4 Discussion

4.1 Offshore transport of dFe and pFe in the Peruvian OMZ

A striking feature of our Fe isotope data is the concurrent shelf-slope plumes of both dissolved (with low δ^{56}dFe) and particulate Fe (with low δ^{56}pFe but higher than δ^{56}dFe), indicative of processes that transport both phases of Fe off shelf (Fig. 3). The distribution of dFe concentrations and Fe isotopic compositions at 12°S are consistent with the iron shuttle process as described for the Peruvian shelf by Scholz et al. (2014). The dFe in the elevated Fe(II) and dFe plumes, with values as low as −1.34‰ in proximity to shelf sediments is consistent with reductive dissolution of Fe from Peruvian shelf sediments. This process acts as an important source of low δ^{56}dFe to overlying seawater where the sediment endmember has been estimated from −0.5 to −1.2‰ (Chever et al., 2015; Scholz et al., 2014; John et al., 2018),

Once released from sediments, Fe(II) is readily oxidized to Fe(III) and subsequently precipitates mainly as isotopically heavier Fe (oxyhydr)oxides in the Peruvian OMZ thus 'shuttling' dFe across the shelf in successive cycles of Fe(II) release followed by precipitation and deposition (Scholz et al., 2014, 2016). In our data, the molar ratios of pFe/pAl along the 12°S transect are significantly elevated relative to the characteristic value of andesitic crust which represents the primary source of terrigenous materials in our study region (Fig. 2a, b and d; Böning et al., 2004; Scholz et al., 2014). These high pFe/pAl ratios indicate accumulation of authigenic Fe originating from substantial precipitation of Fe (oxyhydr)oxides on the inner shelf. Correspondingly, the δ^{56}pFe values (~ −0.2‰) of samples with high pFe/pAl at TM57 are similar to bottom water δ^{56}pFe (~ −0.3‰) reported on the Peruvian inner shelf where Fe (oxyhydr)oxides have been reported to substantially precipitate (Chever et al., 2015; Scholz et al., 2016). Therefore, we propose that enriched pFe in anoxic water column is sourced from Fe (oxyhydr)oxides on the Peruvian inner shelf and transported offshore together with sediment-derived dFe. Our inference is consistent with recent findings on the Oregon margin showing plumes of elevated dFe and pFe extending beyond the shelf-slope break (Floback et al., 2026).

The offshore transport of dFe and pFe observed in our study is distinct from earlier studies at the same region. Along the GEOTRACES GP16 section, which occurred under close to neutral ENSO conditions following a La Niña event earlier in the same year, dFe and pFe were shown to be restricted to the Peruvian inner shelf (Fig. S1). Concentrations of dFe and pFe rapidly decreased below 2 and 10 nmol kg^{-1}, respectively, immediately away from the inner shelf. In contrast, both dFe and pFe in our study were evidently transported across the shelf break (TM56) to the open ocean (TM58) within the anoxic layer (Fig. 3a, b), indicating elevated offshore fluxes of dFe and pFe during M136. The proportion of sediment-derived Fe that is moved offshore (termed horizontal export efficiency hereafter) in coastal upwelling regimes is thought to be related to surface

https://doi.org/10.5194/egusphere-2026-3486
Preprint. Discussion started: 25 June 2026

wind directions and speeds (Siedlecki et al., 2012; Gu et al., 2024). When winds are favorable for upwelling, a larger proportion of sedimentary-derived Fe is transported up the continental shelf slope, resulting in lower horizontal export fluxes to offshore waters (Siedlecki et al., 2012; Gu et al., 2024). Conversely, downwelling-favorable winds increase subsurface stratification and promotes higher offshore export fluxes of sediment-derived Fe. Our cruises were performed during and after the decay phase of the 2017 coastal El Niño event, when wind stress was still low corresponding to sluggish upwelling with rates of 0.01-0.84 m d^{-1} in the mixed layer (Peng et al., 2019; Lüdke et al., 2020; Xie et al., 2020). By contrast, nearshore upwelling rates during GP16 were higher (up to 3 m d^{-1}) (Kadko, 2017). We propose that the difference in upwelling intensity is responsible for the horizontal export efficiency between our study and GP16.

Similar to the 12°S transect, offshore transport of sediment-derived dFe was also evident along 14°S in the OMZ, indicated by a dFe concentration maximum and corresponding lower δ^{56}dFe immediately below the oxic-anoxic interface (Fig. 4). There was also evidence of offshore transport of pFe; however, in contrast to the 12°S transect, the pFe/pAl ratios at 14°S were significantly lower, and are instead similar to those of Peruvian surface sediments and the andesite crustal value (Fig. 2e, f; Taylor and McLennan, 1995). These crust-like pFe/pAl ratios indicate that the elevated pFe at 14°S originates from resuspended sediments from the Peruvian inner shelf potentially under the influences of tides and waves (Becherer et al., 2020; Jefferson et al., 2025). The lack of authigenic Fe signature further implies weaker Fe(II) fluxes from sediment reductive dissolution at 14°S than at 12°S (Rapp et al., 2020). This difference in the magnitude of sedimentary reducing dFe efflux is expected between 12°S and 14°S. 14°S approximates a boundary between a wide continental shelf to the north and a narrow continental shelf to the south. Under similar redox dynamics, broader shelves are generally observed to host higher dFe concentrations (Bruland et al., 2005, Chase et al., 2005) due to the increased exposure of upwelled water masses to sediment dFe effluxes and this trend is evident across all cruises with dFe data from Peru (Gu et al., 2024).

4.2 Drastic variations in offshore fluxes of dFe and pFe at 12°S

A key finding from our study is the drastic decline in dFe and pFe concentrations on the Peruvian shelf at 12°S within a month (Fig. 3a, b). Concentrations of dFe and pFe within the core Fe(II) plume in May 2017 were 3.5 and 10 times, respectively, lower than those one month earlier in April 2017. Correspondingly, δ^{56}dFe increased from −1.34‰ to −0.42‰ (Fig. 3c). During both M136 and M137 cruises, alongshore wind directions were consistent and favorable for weak upwelling (Lüdke et al., 2020; Xie et al., 2020). We thus infer variations in dFe and pFe concentrations to reflect weakened sedimentary reductive dissolution of Fe and, consequently, a significant decrease in the offshore flux of sediment-derived Fe. Strictly, faster Fe(II) oxidation would also have the same effect as reduced gross dFe effluxes from shelf sediments, yet from water column observations only the net efflux of dFe, or Fe(II), can be estimated. A similarly large decrease in dFe at 12°S off Peru has also been documented in Rapp et al. (2020) who attributed these declines to water column oxidation induced by El Niño. However, for our study, both the M136 and M137 campaigns took place in a post El Niño period (Echevin et al., 2018; Rodríguez-Morata et al., 2018). We would expect dFe concentrations to rebound during an El Niño termination, and thus a different mechanism is required to explain the weakened supply of dFe and pFe from the shelf observed during the post El Niño period.

https://doi.org/10.5194/egusphere-2026-3486
Preprint. Discussion started: 25 June 2026

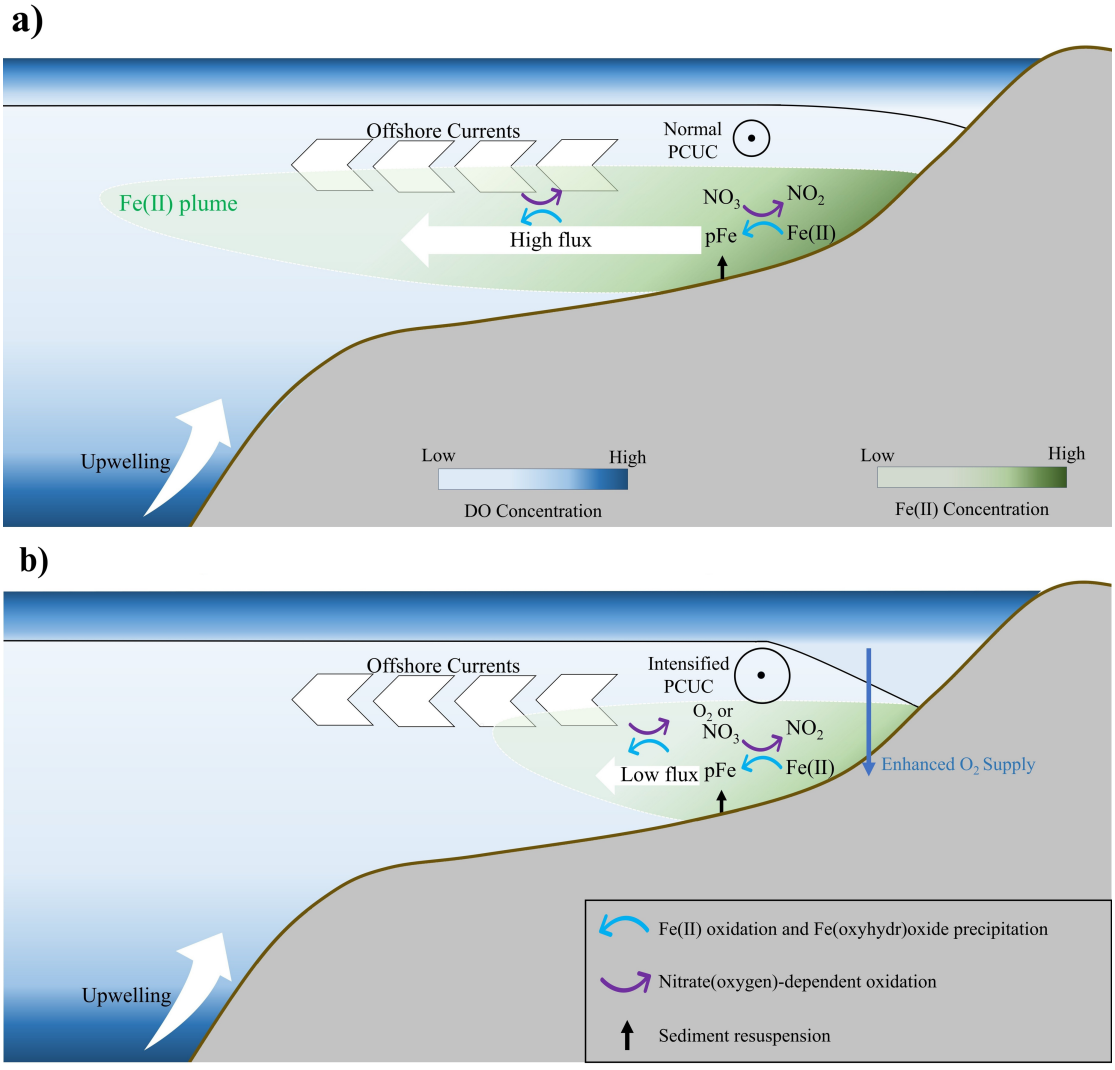

Figure 5. Schematic illustrating the open-marine iron shuttle in the Peruvian OMZ during **a)** normal PCUC and **b)** intensified PCUC scenarios.

In fact, the declines in dFe and pFe observed here at repeat stations in April and May 2017 correspond to the strengthening of the poleward flowing PCUC, with velocities increasing from 0.2 m s^{-1} to 0.5 m s^{-1} (Lüdke et al., 2020). Strengthened PCUC would drive downward displacement of coastal isopycnals and isotherms, and account for a relaxation of coastal nitrogen deficits and bottom water anoxic conditions over the shelf, where bottom water DO concentrations were over 5 µmol kg^{-1} (Lüdke et al., 2020). Such a relief of anoxic conditions over the sediments would reduce release of Fe from reductive sediment dissolution as well as promote Fe re-oxidation, thereby reducing the net porewater-bottom water diffusive flux of Fe(II) (Fig. 5). Our inference is supported by decreased bottom water PO_4 concentrations over the Peruvian shelf during the same sampling campaigns (Lüdke et al., 2020). Phosphate has an affinity to Fe (oxyhydr)oxides in oxic waters, and is desorbed when Fe

https://doi.org/10.5194/egusphere-2026-3486
Preprint. Discussion started: 25 June 2026

(oxyhydr)oxides are dissolved under anoxic conditions, with earlier studies showing concurrent sedimentary release of PO_4 and Fe(II) over the Peruvian anoxic shelf (Noffke et al., 2012; Lomnitz et al., 2016). The temporal variations in Fe and PO_4 concentrations on the shelf, coupled with PCUC intensity, indicate that PCUC plays a key role in regulating Fe(II) effluxes from Peruvian shelf sediments. Variability in diffusive Fe(II) effluxes would influence offshore fluxes and the lateral export efficiency of sediment-derived Fe (Fig. 5).

4.3 Controls on Fe biogeochemistry offshore of the Peruvian slope

Offshore 'within-eddy' crossover stations TM66 and TM75 displayed significantly elevated δ^{56}dFe in the anoxic waters compared to other stations at 12°S, implying little influence from the margin Fe plume at these stations (over 50 km away from the shelf) (Figs. 2 and 3c). This finding is in line with previous studies demonstrating limited exchange of dissolved and particulate constituents across eddy peripheries (Fitzsimmons et al., 2017; Gledhill et al., 2026), so that water column distributions of Fe and δ^{56}Fe are distinctly different between within (eddy stations) and outside the eddy (plume stations). Furthermore, the δ^{56}dFe profiles at TM66 and TM75 were similar to those at offshore stations reported for the eastern section of the GP16 transect (Fitzsimmons et al., 2016; John et al., 2018), both characterized by elevated δ^{56}dFe in the anoxic layer (100-600 m) and lower δ^{56}dFe below (Fig. 6a). Elevated δ^{56}dFe values (−0.05 to +0.73‰) at TM66 and TM75 were accompanied by higher pFe/pAl ratios and low δ^{56}pFe (−0.9 to −0.5‰) (Fig. 2c), also indicative of authigenic formation. Yet, differences in δ^{56}pFe between eddy stations and plume stations ($\Delta\delta^{56}$pFe ~ −0.7 to −0.3‰; Figs. 2a, b and c) suggest that this authigenic Fe formed in offshore waters rather than on the inner shelf. Complexation of dFe by organic ligands, as widely used to explain dFe distributions in the ocean (Gledhill and Buck, 2012) explains a persistent dFe pool, leaving free Fe^{3+} readily precipitating as Fe (oxyhydr)oxides and being scavenged on particles (Tagliabue et al., 2019, 2023; Gledhill et al., 2026). This process facilitates removal of dFe from the water column. Organic ligand binding is thought to concentrate isotopically heavy Fe into the dFe phase (Morgan et al., 2010), in line with the elevated δ^{56}dFe and low δ^{56}pFe observed at depths of 100-600 m at the eddy stations (Fig. 2c).

https://doi.org/10.5194/egusphere-2026-3486
Preprint. Discussion started: 25 June 2026

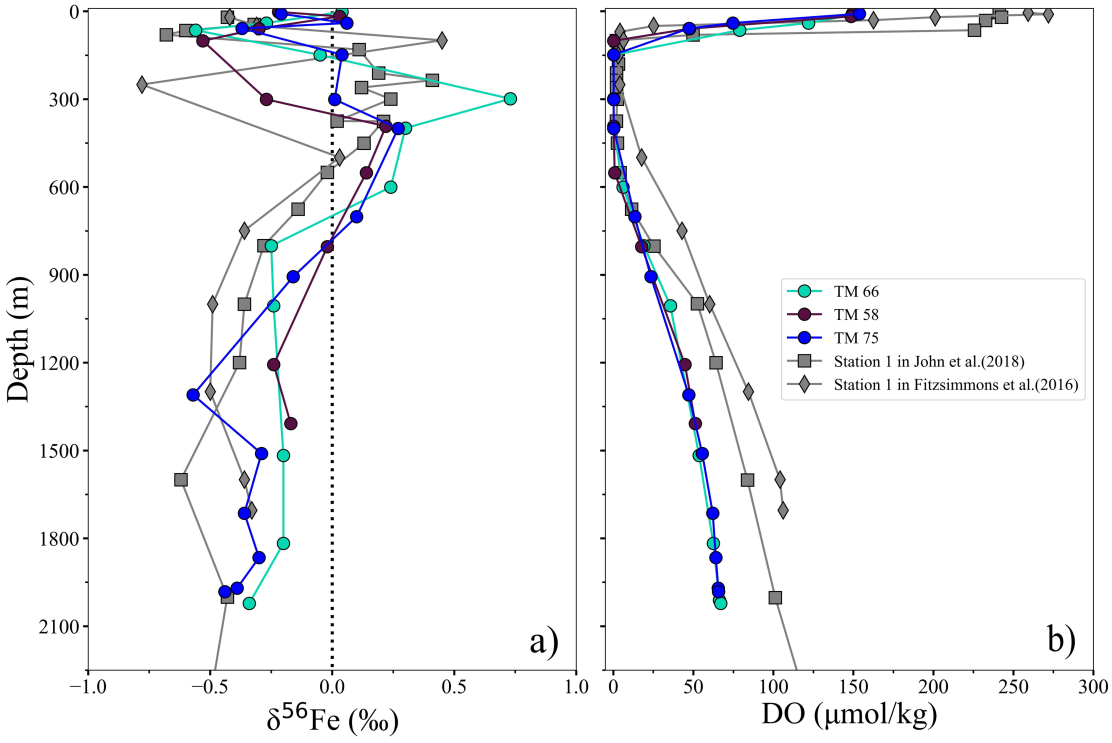

Figure 6. Comparison of **a)** δ^{56}dFe and **b)** DO between offshore stations in our study and in previous studies. The stations in John et al. (2018) and Fitzsimmons et al. (2016) are located respectively at 12°S (Fig. 1) and 20°S off the Peruvian shelf.

We further evaluate whether a reversible scavenging process could account for the δ^{56}dFe profiles observed at the offshore, eddy stations. Reversible scavenging was proposed to account for the presence of an isotopically light, persistent 'slope' dFe plume in the eastern section of the GP16 transect, where particle scavenging was suggested to preferentially remove sediment-derived and isotopically light Fe, resulting in elevated δ^{56}dFe in the anoxic layer, and then subsequent release of this scavenged pFe in the deeper ocean would result in a deep dFe plume (John et al., 2018). However, other recent studies have instead demonstrated that non-reductive (and perhaps reductive) dissolution of sediments on continental slopes are important persistent sources of dFe to the open ocean (Lam et al., 2020; Hunt et al., 2022; Floback et al., 2026). Our study and comparison to other works show that these offshore station locations are consistently not strongly influenced by margin plumes within the anoxic layer. As such, they would be unlikely to sustain a reversible-scavenging system which could then sustain a deep slope plume, instead implying that the dFe below the anoxic layer largely originated from slope sediments. Further, the δ^{56}dFe at slope depths (below 600-800 m) ranging between −0.5‰ and 0‰ off Peru was significantly higher than that derived from reductive dissolution of shelf sediments (Fig. 6a). Sedimentary non-reductive dissolution would be thought to dominate in deeper water with higher oxygen conditions (Homoky et al., 2021), consistent with the increase in DO below 600 m along the Peruvian margin (Fig. 6b). Indeed, previous studies have suggested that such oxic-sediments with lower organic carbon delivery are a

https://doi.org/10.5194/egusphere-2026-3486
Preprint. Discussion started: 25 June 2026

persistent source of non-reductively sourced dFe at slope depths along the Peru margin. However, the δ^{56}dFe of −0.5‰ and 0‰ off Peru indicates both non-reductive and reductive release is important, consistent with δ^{56}dFe signatures as a result of a combination of reductive and non-reductive dissolution of Benguela slope sediments (Hunt et al., 2022). Thus, we conclude that both reductive and non-reductive dissolution of Peruvian slope sediments account for the δ^{56}dFe signatures at slope depths.

5 Conclusions

Our study reveals significant temporal variations in the efficiency of the open-marine Fe shuttle during the El Niño-post El Niño transition in the Peruvian OMZ. In April, 2017, we observed a clear shelf-slope Fe plume within the anoxic layer at 12°S, characterized by elevated Fe(II), dFe and pFe concentrations, and significantly lower δ^{56}dFe and δ^{56}pFe signatures, indicating the predominant contribution of sedimentary reductive dissolution. Such an evident and extensive Fe plume had not been previously reported in the Peruvian upwelling region during GP16. In May, 2017, dFe and pFe concentrations in anoxic layer drastically declined, and δ^{56}dFe was significantly elevated. We attribute these variations to faster-flowing PCUC during a post El Niño period which displaced isotherms downward, bringing in more oxygenated waters and relaxing the release of sediment-derived Fe(II) into the water column. Our study thus highlights the important role of PCUC intensity on Fe isotope biogeochemistry in the Peruvian OMZ. At offshore eddy stations, a combination of organic ligand binding and Fe (oxyhydr)oxide precipitation resulted in elevated δ^{56}dFe and significantly lower δ^{56}pFe in the anoxic layer, while slightly lower δ^{56}dFe below the anoxic layer could be due to lateral supply of sediments experiencing reductive and non-reductive dissolution.

Data availability

All relevant data presented in this study are available in Pangaea at Chen et al. (2026). Cruise CTD data are available in full from Krahmann et al., (2021). Figures 3, 4 and S1 were produced using Ocean Data View (Schlitzer, 2023).

Supplement link

The supplement related to this article includes Figure S1 (GP16 transect of dFe, δ^{56}dFe, and pFe at 12°S off Peru).

Author contributions

Guanghui Chen: conceptualization, visualization, data curation, writing-original draft, review and editing; Insa Rapp: analysis, writing - review and editing; Matthias Sieber: analysis, writing-review and editing; Eric P. Achterberg: funding acquisition, project design, sample collection, writing - review and editing; Tim M. Conway: analysis, writing - review and editing; Martha Gledhill: sample collection, writing - review and editing; Mark J. Hopwood: sample collection, writing-review and editing; Ruifang C. Xie: funding acquisition, project design, methodology, writing-review and editing, supervision.

https://doi.org/10.5194/egusphere-2026-3486
Preprint. Discussion started: 25 June 2026

Competing interests

The authors declare that they have no conflict of interest.

Acknowledgement

We thank the crew and scientific party on board cruises M136, M137 and M138 for their help and support in sample collection. Tim Steffens and Dominik Jasiński are thanked for their laboratory support.

Financial support

Guanghui Chen was supported by the National Science Foundation of China (project number 42376035), Insa Rapp, Eric P. Achterberg, Mark J. Hopwood and Ruifang C. Xie by the German SFB 754 program (project no. 27542298), and Ruifang C. Xie additionally by the NSFC (project number 42376035), German DFG (project number 432469432), the Inge Lehmann Fund and the Shanghai Frontiers Science Center of Polar Science. The cruises were funded by the German SFB 754 program (project no. 27542298).

References

Beard, B. L., Johnson, C. M., Von Damm, K. L., and Poulson, R. L.: Iron isotope constraints on Fe cycling and mass balance in oxygenated Earth oceans. *Geology*, *31*, 629-632, https://doi.org/10.1130/0091-7613(2003)031%3C0629:IICOFC%3E2.0.CO;2, 2003.

Becherer, J., Moum, J. N., Colosi, J. A., Lerczak, J. A., and McSweeney, J. M.: Turbulence asymmetries in bottom boundary layer velocity pulses associated with onshore-propagating nonlinear internal waves. J. Phys. Oceanogr., 50, 2373-2391, https://doi.org/10.1175/JPO-D-19-0178.1, 2020.

Böning, P., Brumsack, H. J., Böttcher, M. E., Schnetger, B., Kriete, C., Kallmeyer, J., and Borchers, S. L.: Geochemistry of Peruvian near-surface sediments. Geochim. Cosmochim. Acta, 68, 4429-4451, https://doi.org/10.1016/j.gca.2004.04.027, 2004.

Browning, T. J., and Moore, C. M.: Global analysis of ocean phytoplankton nutrient limitation reveals high prevalence of co-limitation. Nat. Commun., 14, 5014, https://doi.org/10.1038/s41467-023-40774-0, 2023.

Browning, T. J., Rapp, I., Schlosser, C., Gledhill, M., Achterberg, E. P., Bracher, A., and Le Moigne, F. A. C.: Influence of iron, cobalt, and vitamin B12 supply on phytoplankton growth in the tropical East Pacific during the 2015 El Niño. Geophys. Res. Lett., 45, 6150-6159, https://doi.org/10.1029/2018GL077972, 2018.

Bruland, K. W., Rue, E. L., Smith, G. J., and DiTullio, G. R.: Iron, macronutrients and diatom blooms in the Peru upwelling regime: brown and blue waters of Peru. Mar. Chem., 93, 81-103, https://doi.org/10.1016/j.marchem.2004.06.011, 2005.

https://doi.org/10.5194/egusphere-2026-3486
Preprint. Discussion started: 25 June 2026

Camin, C., Labatut, M., Pradoux, C., Murray, J. W., and Lacan, F.: Iron isotope insights into equatorial Pacific biogeochemistry. Ocean Sci., 22, 791-820, https://doi.org/10.5194/os-22-791-2026, 2026.

Carr, M. E.: Simulation of carbon pathways in the planktonic ecosystem off Peru during the 1997–1998 El Niño and La Niña. J. Geophys. Res., 108, https://doi.org/10.1029/1999JC000064, 2003.

Chaigneau, A., Dominguez, N., Eldin, G., Vasquez, L., Flores, R., Grados, C., and Echevin, V.: Near-coastal circulation in the Northern Humboldt Current System from shipboard ADCP data. J. Geophys. Res. Oceans, 118, 5251-5266, https://doi.org/10.1002/jgrc.20328, 2013.

Chase, Z., Johnson, K. S., Elrod, V. A., Plant, J. N., Fitzwater, S. E., Pickell, L., and Sakamoto, C. M.: Manganese and iron distributions off central California influenced by upwelling and shelf width. Mar. Chem., 95, 235-254, https://doi.org/10.1016/j.marchem.2004.09.006, 2005.

Chavez, F. P., and Messié, M.: A comparison of eastern boundary upwelling ecosystems. Prog. Oceanogr., 83, 80-96, https://doi.org/10.1016/j.pocean.2009.07.032, 2009.

Chen, G., Rapp, I., Sieber, M., Achterberg, E. P., Conway, T. M., Gledhill, M., Hopwood, M. J., Xie, R. C: Dissolved and particulate Fe concentrations and Fe isotope compositions from the Peruvian upwelling zone (M136 to M138) [dataset]. PANGAEA, https://doi.pangaea.de/10.1594/PANGAEA.995338, 2026.

Chever, F., Rouxel, O. J., Croot, P. L., Ponzevera, E., Wuttig, K., and Auro, M.: Total dissolvable and dissolved iron isotopes in the water column of the Peru upwelling regime. Geochim. Cosmochim. Acta, 162, 66-82, https://doi.org/10.1016/j.gca.2015.04.031, 2015.

Conway, T. M., and John, S. G.: Quantification of dissolved iron sources to the North Atlantic Ocean. Nature, 511, 212-215, https://doi.org/10.1038/nature13482, 2014.

Conway, T. M., John, S. G., and Lacan, F.: Intercomparison of dissolved iron isotope profiles from reoccupation of three GEOTRACES stations in the Atlantic Ocean. Mar. Chem., 183, 50-61, https://doi.org/10.1016/j.marchem.2016.04.007, 2016.

Conway, T. M., Rosenberg, A. D., Adkins, J. F., and John, S. G.: A new method for precise determination of iron, zinc and cadmium stable isotope ratios in seawater by double-spike mass spectrometry. Anal. Chim. Acta, 793, 44-52, https://doi.org/10.1016/j.aca.2013.07.025, 2013.

Echevin, V., Colas, F., Espinoza-Morriberon, D., Vasquez, L., Anculle, T., and Gutierrez, D.: Forcings and evolution of the 2017 coastal El Niño off Northern Peru and Ecuador. Front. Mar. Sci., 5, 367, https://doi.org/10.3389/fmars.2018.00367, 2018.

Espinoza-Morriberón, D., Echevin, V., Colas, F., Tam, J., Ledesma, J., Vásquez, L., and Graco, M.: Impacts of El Niño events on the Peruvian upwelling system productivity. J. Geophys. Res. Oceans, 122, 5423-5444, https://doi.org/10.1002/2016JC012439, 2017.

https://doi.org/10.5194/egusphere-2026-3486
Preprint. Discussion started: 25 June 2026

Fitzsimmons, J. N., Conway, T. M., Lee, J. M., Kayser, R., Thyng, K. M., John, S. G., and Boyle, E. A.: Dissolved iron and iron isotopes in the southeastern Pacific Ocean. Global Biogeochem. Cycles, 30, 1372-1395, https://doi.org/10.1002/2015GB005357, 2016.

Fitzsimmons, J. N., and Conway, T. M.: Novel insights into marine iron biogeochemistry from iron isotopes. Annu. Rev. Mar. Sci., 15, 383-406, https://doi.org/10.1146/annurev-marine-032822-103431, 2023.

Fitzsimmons, J. N., John, S. G., Marsay, C. M., Hoffman, C. L., Nicholas, S. L., Toner, B. M., and German, C. R.: Iron persistence in a distal hydrothermal plume supported by dissolved–particulate exchange. Nat. Geosci., 10, 195-201, https://doi.org/10.1038/ngeo2900, 2017.

Floback, A. E., Pham, A. L. D., Damien, P., Odendahl, C. E., Weiske, J., Thomas, K. E., Bianchi, D., and Moffett, J. W.: Iron supply from the Oregon margin to the ocean dominated by hypoxia-dependent particles. Proc. Natl. Acad. Sci. USA, 123, e2532929123, https://doi.org/10.1073/pnas.2532929123, 2026.

Froelich, P. N., Klinkhammer, G. P., Bender, M. L., Luedtke, N. A., Heath, G. R., Cullen, D., Dauphin, P., Hammond, D., Hartman, B., and Maynard, V.: Early oxidation of organic matter in pelagic sediments of the eastern equatorial Atlantic: suboxic diagenesis. Geochim. Cosmochim. Acta, 43, 1075-1090, https://doi.org/10.1016/0016-7037(79)90095-4, 1979.

Garcia H.E., Wang Z., Bouchard C., Cross S.L., Paver C.R., Reagan J.R., Boyer T.P., Locarnini R.A., Mishonov A.V., Baranova O.K., Seidov D., Dukhovskoy D.: WORLD OCEAN ATLAS 2023. Volume 3: Dissolved Oxygen, Apparent Oxygen Utilization, Dissolved Oxygen Saturation, and 30-year Climate Normal. Ref. NOAA Atlas NESDIS 91. 109p.. NOAA. https://doi.org/10.25923/rb67-ns53, 2024.

Gledhill, M., and Buck, K. N.: The organic complexation of iron in the marine environment: a review. Front. Microbiol., 3, 69, https://doi.org/10.3389/fmicb.2012.00069, 2012.

Gledhill, M., Gosnell, K., Humphreys, M. P., Delaigue, L., Helle, N., Zhu, K., Lodeiro, P., Rey-Castro, C., and Achterberg, E. P.: Chemical controls on iron distributions across the subsurface South Pacific Ocean. Nat. Commun., 17, 3533, https://doi.org/10.1038/s41467-026-72070-y, 2026.

Gong, Y., Xia, Y., Huang, F., and Yu, H.: Average iron isotopic compositions of the upper continental crust: constrained by loess from the Chinese Loess Plateau. Acta Geochim., 36, 125-131, https://doi.org/10.1007/s11631-016-0131-5, 2017.

Gu, Y., Hopwood, M. J., Gledhill, M., Rapp, I., Wuttig, K., and Achterberg, E. P.: Spatial and temporal variations in the micronutrient Fe across the Peruvian shelf from 1984 to 2017. Prog. Oceanogr., 221, 103208, https://doi.org/10.1016/j.pocean.2024.103208, 2024.

Heller, M. I., Lam, P. J., Moffett, J. W., Till, C. P., Lee, J. M., Toner, B. M., and Marcus, M. A.: Accumulation of Fe oxyhydroxides in the Peruvian oxygen deficient zone implies non-oxygen dependent Fe oxidation. Geochim. Cosmochim. Acta, 211, 174-193, https://doi.org/10.1016/j.gca.2017.05.019, 2017.

https://doi.org/10.5194/egusphere-2026-3486
Preprint. Discussion started: 25 June 2026

Homoky, W. B., Conway, T. M., John, S. G., König, D., Deng, F., Tagliabue, A., and Mills, R. A.: Iron colloids dominate sedimentary supply to the ocean interior. Proc. Natl. Acad. Sci. USA, 118, e2016078118, https://doi.org/10.1073/pnas.2016078118, 2021.

Homoky, W. B., John, S. G., Conway, T. M., and Mills, R. A.: Distinct iron isotopic signatures and supply from marine sediment dissolution. Nat. Commun., 4, 2143, https://doi.org/10.1038/ncomms3143, 2013.

Homoky, W. B., Severmann, S., Mills, R. A., Statham, P. J., and Fones, G. R.: Pore-fluid Fe isotopes reflect the extent of benthic Fe redox recycling: evidence from continental shelf and deep-sea sediments. Geology, 37, 751-754, https://doi.org/10.1130/G25731A.1, 2009.

Hunt, H. R.: Isotopic Fingerprints of the Coastal Margins: Tracing Dissolved Iron Sources from Land to Sea. Ph.D. thesis, University of South Florida, 2025.

Hunt, H. R., Summers, B. A., Sieber, M., Krisch, S., Al-Hashem, A., Hopwood, M., Achterberg, E. P., Lodeiro, P., and Fietz, S.: Distinguishing the influence of sediments, the Congo River, and water-mass mixing on the distribution of iron and its isotopes in the Southeast Atlantic Ocean. Mar. Chem., 247, 104181, https://doi.org/10.1016/j.marchem.2022.104181, 2022.

Hutchins, D. A., Hare, C. E., Weaver, R. S., Zhang, Y., Firme, G. F., DiTullio, G. R., Alm, M. B., Riseman, S. F., Maucher, J. M., Geesey, M. E., Trick, C. G., Smith, G. J., Rue, E. L., Conn, J., and Bruland, K. W.: Phytoplankton iron limitation in the Humboldt Current and Peru Upwelling. Limnol. Oceanogr., 47, 997-1011, https://doi.org/10.4319/lo.2002.47.4.0997, 2002.

Jefferson, J., Simeonov, J., Calantoni, J., and Sheremet, A.: Sediment Resuspension on the Inner Shelf under Combined Internal Tides and Waves and Surface Waves: Field Observations and Modeling. J. Phys. Oceanogr., 55, 941-957, https://doi.org/10.1175/JPO-D-24-0081.1, 2025.

John, S. G., Helgoe, J., Townsend, E., Weber, T., DeVries, T., Tagliabue, A., Moore, K., Lam, P., Marsay, C. M., and Till, C.: Biogeochemical cycling of Fe and Fe stable isotopes in the Eastern Tropical South Pacific. Mar. Chem., 201, 66-76, https://doi.org/10.1016/j.marchem.2017.06.003, 2018.

John, S. G., Mendez, J., Moffett, J., and Adkins, J.: The flux of iron and iron isotopes from San Pedro Basin sediments. Geochim. Cosmochim. Acta, 93, 14-29, https://doi.org/10.1016/j.gca.2012.06.019, 2012.

José, Y. S., Stramma, L., Schmidtko, S., and Oschlies, A.: ENSO-driven fluctuations in oxygen supply and vertical extent of oxygen-poor waters in the oxygen minimum zone of the Eastern Tropical South Pacific. Biogeosciences, 16, 3987-4006, https://doi.org/10.5194/bg-16-3987-2019, 2019.

Kadko, D.: Upwelling and primary production during the U.S. GEOTRACES East Pacific Zonal Transect. Global Biogeochem. Cycles, 31, 218-232, https://doi.org/10.1002/2016GB005554, 2017.

Karstensen, J., Stramma, L., and Visbeck, M.: Oxygen minimum zones in the eastern tropical Atlantic and Pacific oceans. Prog. Oceanogr., 77, 331-350, https://doi.org/10.1016/j.pocean.2007.05.009, 2008.

https://doi.org/10.5194/egusphere-2026-3486
Preprint. Discussion started: 25 June 2026

Klar, J. K., Homoky, W. B., Statham, P. J., Birchill, A. J., Harris, E. L., Woodward, E. M. S., Silburn, B., Cooper, M. J., James, R. H., Connelly, D. P., Chever, F., Lichtschlag, A., and Graves, C.: Stability of dissolved and soluble Fe(II) in shelf sediment pore waters and release to an oxic water column. Biogeochemistry, 135, 49-67, https://doi.org/10.1007/s10533-017-0309-x, 2017.

Kurisu, M., Sakata, K., Nishioka, J., Obata, H., Conway, T. M., Hunt, H. R., Sieber, M., Suzuki, K., Kashiwabara, T., Kubo, S., Takada, M., and Takahashi, Y.: Source and fate of atmospheric iron supplied to the subarctic North Pacific traced by stable iron isotope ratios. Geochim. Cosmochim. Acta, 378, 168-185, https://doi.org/10.1016/j.gca.2024.06.009, 2024.

Krahmann, G., Arévalo-Martínez, D. L., Dale, A. W., Dengler, M., Engel, A., Glock, N., et al.: Krahmann, G., Arévalo-Martínez, D. L., Dale, A. W., Dengler, M., Engel, A., Glock, N., Hauss, H., Körtzinger, A., Lüdke, J., Montoya, J. P., M., D., Sommer, S., Stramma, L., and Thomsen, S.: Climate-Biogeochemistry Interactions in the Tropical Ocean: Data Collection and Legacy. Front. Mar. Sci., 8, 723304, https://doi.org/10.3389/fmars.2021.723304, 2021.

Lam, P. J., Heller, M. I., Lerner, P. E., Moffett, J. W., and Buck, K. N.: Unexpected Source and Transport of Iron from the Deep Peru Margin. ACS Earth Space Chem., 4, 977-992, https://doi.org/10.1021/acsearthspacechem.0c00066, 2020.

Liu, X., and Millero, F. J.: The solubility of iron in seawater. Mar. Chem., 77, 43-54, https://doi.org/10.1016/S0304-4203(01)00074-3, 2002.

Lomnitz, U., Sommer, S., Dale, A. W., Löscher, C. R., Noffke, A., Wallmann, K., and Hensen, C.: Benthic phosphorus cycling in the Peruvian oxygen minimum zone. Biogeosciences, 13, 1367-1386, https://doi.org/10.5194/bg-13-1367-2016, 2016.

Lüdke, J., Dengler, M., Sommer, S., Clemens, D., Thomsen, S., Krahmann, G., and Dale, A. W.: Influence of intraseasonal eastern boundary circulation variability on hydrography and biogeochemistry off Peru. Ocean Sci., 16, 1347-1366, https://doi.org/10.5194/os-16-1347-2020, 2020.

Miller, W. L., King, D. W., Lin, J., and Kester, D. R.: Photochemical redox cycling of iron in coastal seawater. Mar. Chem., 50, 63-77, https://doi.org/10.1016/0304-4203(95)00029-F, 1995.

Morel, F. M. M., and Price, N. M.: The biogeochemical cycles of trace metals in the oceans. Science, 300, 944-947, https://doi.org/10.1126/science.1083545, 2003.

Morgan, J. L., Wasylenki, L. E., Nuester, J., and Anbar, A. D.: Fe isotope fractionation during equilibration of Fe-organic complexes. Environ. Sci. Technol., 44, 6095-6101, https://doi.org/10.1021/es101167w, 2010.

Noffke, A., Hensen, C., Sommer, S., Scholz, F., Bohlen, L., Mosch, T., Graco, M., and Wallmann, K.: Benthic iron and phosphorus fluxes across the Peruvian oxygen minimum zone. Limnol. Oceanogr., 57, 851-867, https://doi.org/10.4319/lo.2012.57.3.0851, 2012.

Peng, Q., Xie, S. P., Wang, D., Zheng, X. T., and Zhang, H.: Coupled ocean-atmosphere dynamics of the 2017 extreme coastal El Niño. Nat. Commun., 10, 298, https://doi.org/10.1038/s41467-018-08258-8, 2019.

Pauly, D., and Christensen, V.: Primary production required to sustain global fisheries. Nature, 374, 255-257, https://doi.org/10.1038/374255a0, 1995.

https://doi.org/10.5194/egusphere-2026-3486
Preprint. Discussion started: 25 June 2026

Ramírez, I. J., and Briones, F.: Understanding the El Niño Costero of 2017: The Definition Problem and Challenges of Climate Forecasting and Disaster Responses. Int. J. Disaster Risk Sci., 8, 489-492, https://doi.org/10.1007/s13753-017-0151-7, 2017.

Rapp, I., Schlosser, C., Browning, T. J., Wolf, F., Le Moigne, F. A., Gledhill, M., Achterberg, E. P., and Engel, A.: El Niño-Driven Oxygenation Impacts Peruvian Shelf Iron Supply to the South Pacific Ocean. Geophys. Res. Lett., 47, e2019GL086631, https://doi.org/10.1029/2019GL086631, 2020.

Rodríguez-Morata, C., Díaz, H. F., Ballesteros-Canovas, J. A., Rohrer, M., and Stoffel, M.: The anomalous 2017 coastal El Niño event in Peru. Clim. Dyn., 52, 5605-5622, https://doi.org/10.1007/s00382-018-4460-3, 2019.

Schlitzer, R.: Ocean Data View, https://odv.awi.de, 2023.

Schlosser, C., Streu, P., Frank, M., Lavik, G., Croot, P. L., Dengler, M., and Achterberg, E. P.: H_2S events in the Peruvian oxygen minimum zone facilitate enhanced dissolved Fe concentrations. Sci. Rep., 8, 12642, https://doi.org/10.1038/s41598-018-30580-w, 2018.

Scholz, F., Hensen, C., Noffke, A., Rohde, A., Liebetrau, V., and Wallmann, K.: Early diagenesis of redox-sensitive trace metals in the Peru upwelling area–response to ENSO-related oxygen fluctuations in the water column. Geochim. Cosmochim. Acta, 75, 7257-7276, https://doi.org/10.1016/j.gca.2011.08.007, 2011.

Scholz, F., Löscher, C. R., Fiskal, A., Sommer, S., Hensen, C., Lomnitz, U., Wuttig, K., Göttlicher, J., Kossel, E., Steininger, F. F., and Canfield, D. E.: Nitrate-dependent iron oxidation limits iron transport in anoxic ocean regions. Earth Planet. Sci. Lett., 454, 272-281, https://doi.org/10.1016/j.epsl.2016.09.025, 2016.

Scholz, F., Severmann, S., McManus, J., and Hensen, C.: Beyond the Black Sea paradigm: the sedimentary fingerprint of an open-marine iron shuttle. Geochim. Cosmochim. Acta, 127, 368-380, https://doi.org/10.1016/j.gca.2013.11.041, 2014.

Severmann, S., McManus, J., Berelson, W. M., and Hammond, D. E.: The continental shelf benthic iron flux and its isotope composition. Geochim. Cosmochim. Acta, 74, 3984-4004, https://doi.org/10.1016/j.gca.2010.04.022, 2010.

Severmann, S., Johnson, C. M., Beard, B. L., and McManus, J.: The effect of early diagenesis on the Fe isotope compositions of porewaters and authigenic minerals in continental margin sediments. Geochim. Cosmochim. Acta, 70, 2006-2022, https://doi.org/10.1016/j.gca.2006.01.007, 2006.

Sieber, M., Conway, T. M., de Souza, G. F., Hassler, C. S., Ellwood, M. J., and Vance, D.: Isotopic fingerprinting of biogeochemical processes and iron sources in the iron-limited surface Southern Ocean. Earth Planet. Sci. Lett., 567, 116967, https://doi.org/10.1016/j.epsl.2021.116967, 2021.

Sieber, M., Lanning, N. T., Steffen, J. M., Bian, X., Yang, S. C., Lee, J., Hatta, M., Aguilar-Islas, A., Firing, E., Rember, R., Zhang, R., Bundy, R. M., Lethaby, P., and Wu, J.: Long distance transport of subsurface sediment-derived iron from Asian to Alaskan margins in the North Pacific Ocean. Geophys. Res. Lett., 51, e2024GL110836, https://doi.org/10.1029/2024GL110836, 2024.

Siedlecki, S. A., Mahadevan, A., and Archer, D. E.: Mechanism for export of sediment-derived iron in an upwelling regime. Geophys. Res. Lett., 39, L03601, https://doi.org/10.1029/2011GL050366, 2012.

https://doi.org/10.5194/egusphere-2026-3486
Preprint. Discussion started: 25 June 2026

Stramma, L., Fischer, T., Grundle, D. S., Krahmann, G., Bange, H. W., and Marandino, C. A.: Observed El Niño conditions in the eastern tropical Pacific in October 2015. Ocean Sci., 12, 861-873, https://doi.org/10.5194/os-12-861-2016, 2016.

Tagliabue, A., Bowie, A. R., DeVries, T., Ellwood, M. J., Landing, W. M., Milne, A., Ohnemus, D. C., Twining, B. S., and Boyd, P. W.: The interplay between regeneration and scavenging fluxes drives ocean iron cycling. Nat. Commun., 10, 4960, https://doi.org/10.1038/s41467-019-12775-5, 2019.

Tagliabue, A., Buck, K. N., Sofen, L. E., Twining, B. S., Aumont, O., Boyd, P. W., Caprara, S., Harrison, C. S., Hirst, C. A., Ohnemus, D. C., Robidart, J. C., and Schanke, N. L.: Authigenic mineral phases as a driver of the upper-ocean iron cycle. Nature, 620, 104-109, https://doi.org/10.1038/s41586-023-06210-5, 2023.

Taylor, S. R., and McLennan, S. M.: The geochemical evolution of the continental crust. Rev. Geophys., 33, 241-265, https://doi.org/10.1029/95RG00262, 1995.

Tian, H. A., van Manen, M., Bunnell, Z. B., Jung, J., Lee, S. H., Kim, T. W., Conway, T. M., and Middag, R.: Biogeochemistry of iron in coastal Antarctica: isotopic insights for external sources and biological uptake in the Amundsen Sea polynyas. Geochim. Cosmochim. Acta, 363, 51-67, https://doi.org/10.1016/j.gca.2023.10.029, 2023.

Tian, H. A., van Manen, M., Bunnell, Z. B., Reichart, G. J., Conway, T. M., and Middag, R.: Iron isotope constraints on source and transport of sediment-derived dissolved Fe in the Weddell Sea region. Geochim. Cosmochim. Acta, 417, 122-134, https://doi.org/10.1016/j.gca.2026.01.033, 2026.

Vedamati, J., Goepfert, T., and Moffett, J. W.: Iron speciation in the eastern tropical South Pacific oxygen minimum zone off Peru. Limnol. Oceanogr., 59, 1945-1957, https://doi.org/10.4319/lo.2014.59.6.1945, 2014.

Whitfield, M.: Interactions between phytoplankton and trace metals in the ocean, in Advances in Marine Biology, edited by Southward, A. J., Young, C. M., Tyler, P. A., Fuiman, L. A., Academic Press, New York, 3-120, https://hero.epa.gov/reference/8151879/, 2001.

Xie, R. C., Le Moigne, F. A. C., Rapp, I., Lüdke, J., Gasser, B., Dengler, M., Liebetrau, V., and Achterberg, E. P.: Effects of ^{238}U variability and physical transport on water column ^{234}Th downward fluxes in the coastal upwelling system off Peru. Biogeosciences, 17, 4919-4936, https://doi.org/10.5194/bg-17-4919-2020, 2020.

Zhu, K., Hopwood, M. J., Groenenberg, J. E., Engel, A., Achterberg, E. P., and Gledhill, M.: Influence of pH and dissolved organic matter on iron speciation and apparent iron solubility in the Peruvian shelf and slope region. Environ. Sci. Technol., 55, 9372-9383, https://doi.org/10.1021/acs.est.1c02477, 2021.